OXFORD

Human Molecular Genetics, 2016, Vol. 25, No. 19 4186–4200

doi: 10.1093/hmg/ddw252
Advance Access Publication Date: 27 July 2016
Original Article

ORIGINAL ARTICLE

A mouse model for creatine transporter deficiency reveals early onset cognitive impairment and neuropathology associated with brain aging

Laura Baroncelli[1,*], Angelo Molinaro[1,2], Francesco Cacciante[3], Maria Grazia Alessandrì[4], Debora Napoli[3], Elena Putignano[1], Jonida Tola[1], Vincenzo Leuzzi[5], Giovanni Cioni[4,6] and Tommaso Pizzorusso[1,2]

[1]Institute of Neuroscience, National Research Council (CNR), Pisa, Italy, [2]Department of Neuroscience, Psychology, Drug Research and Child Health NEUROFARBA, University of Florence, Florence, Italy, [3]BioSNS laboratory, Scuola Normale Superiore di Pisa, Pisa, Italy, [4]Department of Developmental Neuroscience, IRCCS Stella Maris Scientific Institute, IRCCS Stella Maris Foundation, Pisa, Italy, [5]Department of Paediatrics, Child Neurology and Psychiatry, Sapienza University of Rome, Rome, Italy and [6]Department of Clinical and Experimental Medicine, University of Pisa, Pisa, Italy

*To whom correspondence should be addressed at: Laura Baroncelli, Institute of Neuroscience, National Research Council (CNR) via Moruzzi 1, Pisa I-56124, Italy. Tel: +390 503 153199; Fax: +390 503 153220; Email: baroncelli@in.cnr.it

Abstract

Mutations in the creatine (Cr) transporter (CrT) gene lead to cerebral creatine deficiency syndrome-1 (CCDS1), an X-linked metabolic disorder characterized by cerebral Cr deficiency causing intellectual disability, seizures, movement and autistic-like behavioural disturbances, language and speech impairment. Since no data are available about the neural and molecular underpinnings of this disease, we performed a longitudinal analysis of behavioural and pathological alterations associated with CrT deficiency in a CCDS1 mouse model. We found precocious cognitive and autistic-like defects, mimicking the early key features of human CCDS1. Moreover, mutant mice displayed a progressive impairment of short and long-term declarative memory denoting an early brain aging. Pathological examination showed a prominent loss of GABAergic synapses, marked activation of microglia, reduction of hippocampal neurogenesis and the accumulation of autofluorescent lipofuscin. Our data suggest that brain Cr depletion causes both early intellectual disability and late progressive cognitive decline, and identify novel targets to design intervention strategies aimed at overcoming brain CCDS1 alterations.

Introduction

Creatine (Cr) has a fundamental role in the energy metabolism of cells, particularly in tissues with high-energy demand. Cr kinase (CK) catalyzes the reversible conversion of Cr and ATP to phosphoCr (PCr) and ADP. Most of the cells, indeed, do not rely on ATP/ADP free diffusion and the CK/PCr/Cr system serves as energy storage for immediate regeneration of ATP and as shuttle of high-energy phosphates between sites of ATP production and consumption (1). In physiological conditions, Cr is obtained by diet and by endogenous synthesis, which involves the enzymes l-arginine:glycineamidinotransferase (AGAT) and S-adenosyl-l-methionine:N-guanidinoacetatemethyltransferase

Received: June 19, 2016. **Revised:** July 17, 2016. **Accepted:** July 18, 2016

(GAMT). Additionally, Cr is a polar hydrophilic molecule unable to cross the plasma membrane and a specific Na^+/Cl^--dependent transporter (Cr transporter, CrT) is required for Cr to enter the cells (2).

The great relevance of Cr/PCr system for the normal functioning of brain cells is well supported by the recent discovery of three different pathologies characterized by defects of Cr metabolism that lead to primary neurological symptoms. AGAT (3) and GAMT disorders (4) are autosomal recessive conditions impairing Cr biosynthesis, while CrT deficiency (CCDS1) is an X-linked condition affecting cellular uptake of Cr (5). These disorders share the depletion of brain Cr and a similar clinical phenotype with intellectual disability, behavioural autistic-like abnormalities, language and speech disturbances, seizures and movement disorders (2,6). Very little is known about Cr regulation and function in the brain. In the central nervous system, AGAT, GAMT and CrT are widely expressed in brain cells, including neurons, oligodendrocytes, and endothelial cells of the blood-brain barrier (7,8).

The lack of knowledge about the effects of Cr deficiency on neuronal circuits stems at least partially from the paucity of studies on animal models. Two germline murine models of CCDS1 and one model of GAMT deficiency are available so far (9–11), and they have been analysed only in some behavioural domains and at neurochemical level, while studies on AGAT-deficient mice are limited to metabolic effects of Cr deficiency (12). Learning and memory deficits, impaired motor activity and Cr depletion in the brain and muscles have been reported in GAMT and CrT models in the adult age (9–11). However, little is known about the presence of autistic-like behavioural features and the onset and progression of the phenotype.

Several papers found that the disturbed energy metabolism caused by prolonged and sustained Cr depletion might resonate in molecular networks resulting in abnormal metabolism. Accordingly, the skeletal muscle of AGAT deficient mice displays a marked increase of inorganic phosphate/ATP ratio and overall mitochondrial content, while ATP levels were reduced by nearly half (13). Patients with Cr deficiency syndrome are reported to have increased oxidative stress and reactive oxygen species (ROS)-induced apoptotic cell loss (14), whereas Cr supplementation in senescent mice improved neurobehavioural outcomes and prolonged median survival with a trend towards lower ROS (15). We speculated that the disturbed energy metabolism caused by prolonged and sustained Cr depletion might set in motion the precocious activation of detrimental cellular and molecular mechanisms typical of brain aging leading to a progressive cognitive regression. The lack of the antioxidant activity of Cr (16,17) in CCDS1 might also contribute to this process (18). This hypothesis would explain the observation that intellectual disability of CCDS1 patients seems to become more pronounced with age (19). Intriguingly, our surmise could also be relevant for normal brain aging as suggested by recent data showing that Cr levels are downregulated in the aged human brain (20,21).

Thus, we performed a longitudinal evaluation of cognitive functions in CrT deficient mice and we examined various age-related brain phenotypes including neuronal degeneration, hippocampal neurogenesis, synaptic loss, neuroinflammation and oxidative stress. Our results show that reduced Cr levels accelerate the brain aging process, indicating that CCDS1 could be considered an age-dependent disorder and that alterations of Cr metabolism are directly involved in brain aging.

Results

Reduced body weight growth in $CrT^{-/y}$ mice

A first clue indicating that CrT deficiency elicits age-related detrimental effects emerged from the general appearance of mutant animals. Mice were weighed at different ages and compared with WT littermates. Even though no particular problems of breeding were observed and the face of $CrT^{-/y}$ mice was normal till P40, $CrT^{-/y}$ animals ($n = 12$) showed a significantly reduced body weight compared to $CrT^{+/y}$ animals at P60, P100 and P180 ($n = 13$; Two way ANOVA on rank transformed data, $P < 0.001$ effect of genotype, $P < 0.001$ interaction between genotype and age; post hoc Holm Sidak method, $P = 0.092$ at P40, $P < 0.001$ in all other comparisons; Supplementary Material, Fig. S1).

Age-related deterioration of cognitive functions in Cr deficiency conditions

In a previous behavioural investigation performed at P40, we highlighted that $CrT^{-/y}$ mice exhibit a general cognitive impairment across different learning and memory tests (11). To understand whether a progressive deterioration of behavioural impairment is present in $CrT^{-/y}$ mice, we studied four different stages: 1. during the early brain development (postnatal day (P) 28 at the beginning of testing), 2. during the late brain development (P40 at the beginning of testing), 3. in the adult age (P100 at the beginning of testing), and 4. in the middle age (P180 at the beginning of testing). Interestingly, a progressive worsening of cognitive symptoms was detectable in $CrT^{-/y}$ mutant mice, suggesting that age is a key feature of Cr deficiency disease.

Y *maze*

We first analysed the performance of $CrT^{-/y}$ animals at P28 using the Y maze spontaneous alternation, which is an optimal task for probing memory in juveniles (Fig. 1A; 22). Animals of both groups equally explored all the three arms of the maze. Indeed, no effect of genotype was detected for either the number of entries in the single arms of the maze (designated A, B, C) or the total number of arm entries, indicating that the exploratory disposition of mutant animals ($n = 9$) was not altered compared to WT littermates ($n = 11$; Two-Way ANOVA on rank transformed data, post hoc Holm-Sidak method, $P = 0.506$, $P = 0.941$, $P = 0.276$, $P = 0.391$ respectively, Fig. 1A). However, while in young WT mice alternation rate was about 60% of total arm choices, in $CrT^{-/y}$ animals it dropped to the chance level (50%; Fig. 1B), demonstrating that CrT disruption in the mouse model could reproduce the early pathological phenotype of CCDS1 patients. The same impairment was detected at P40, P100 and P180 with $CrT^{-/y}$ mice performing at chance level whereas WT age-matched controls showed significant spontaneous alternation (t-test, $P < 0.01$ for P40, $P < 0.05$ for P100 and P180, Supplementary Material, Fig. S2). These data also indicated that the spontaneous alternation paradigm cannot reveal age-dependent cognitive decline in CrT mutants because of the ceiling effect in the arm alternation deficit masking the effect of the age variable.

Object recognition test (ORT)

We assessed declarative memory abilities in the ORT, a test based on the spontaneous tendency of rodents to spend more time exploring a novel object than a familiar one. No difference in short-term recognition memory between P40 $CrT^{-/y}$ mice

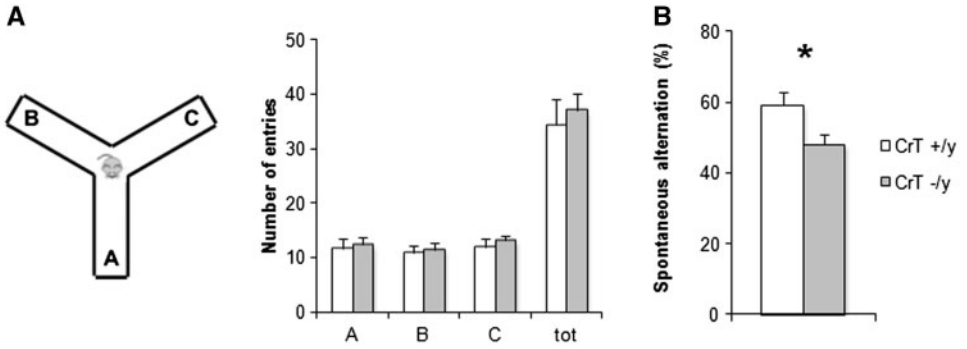

Figure 1. Early deficiency of working memory in $CrT^{-/y}$ mice. (**A**) Schematic diagram of the Y maze apparatus. The mean number of entries in the single arms of the maze (**A, B, C**) and the total number of arm entries were comparable for the different experimental groups (Two-Way ANOVA on rank transformed data, post hoc Holm-Sidak method, $P = 0.506$, $P = 0.941$, $P = 0.276$, $P = 0.391$, respectively). (B) Alternation rate in the Y maze was significantly lower in $CrT^{-/y}$ mice ($n = 9$) compared to that recorded for $CrT^{+/y}$ littermates ($n = 11$; t test, $P < 0.05$) at P28. *$P < 0.05$. Error bars, s.e.m.

($n = 9$) and age-matched WT animals ($n = 7$) could be detected (*t*-test, $P = 0.285$). In contrast, the discrimination index at 24 h was significantly lower in mutant mice, indicating that their capacity to recall the familiar object was impaired (*t*-test, $P < 0.05$; Fig. 2A). This memory deficit became more pronounced two months later ($CrT^{-/y}$ $n = 11$, $CrT^{+/y}$ $n = 10$; P100, *t*-test, $P < 0.01$ at 24h; Fig. 2B), eventually affecting both short- and long-term memories at P180. Indeed, at P180 $CrT^{-/y}$ mice showed a marked memory deficit both at 1- and 24-h interval between the sample and the test phase with respect to $CrT^{+/y}$ mice ($CrT^{-/y}$ $n = 10$, $CrT^{+/y}$ $n = 9$; *t*-test, $P < 0.05$ for both comparisons; Fig. 2C), indicating that the longer the time during which neural circuits are forced to work without Cr energy buffer the worse the cognitive performance of $CrT^{-/y}$ animals.

Morris water maze (MWM)

We further assessed memory abilities in the MWM, a cognitive paradigm that allows testing spatial learning and memory. The probe test highlighted a spatial memory impairment in Cr deficient mice at all the different ages tested: WT animals, indeed, spent significantly longer time in the quadrant where the platform was located during the training days (NE*; Two-Way RM ANOVA, post hoc Holm-Sidak method, $P < 0.05$ for all comparisons), while mutant mice did not remember the location of the hidden platform and equally explored the four quadrants of the maze (Two-Way RM ANOVA, post hoc Holm-Sidak method; Supplementary Material, Fig. S3).

The results obtained in the training phase of the MWM test, however, showed a clear progression of cognitive deficits in $CrT^{-/y}$ mice. Since a main effect of genotype was found on mean swimming speed recorded all along the training phase at the different ages tested (t-test, $P < 0.05$ (P40); Mann–Whitney Rank Sum test, $P < 0.05$ (P100); *t*-test, $P < 0.01$ (P180); Supplementary Material, Fig. S4), we analysed the length of path covered to find the submerged platform. At P40 $CrT^{-/y}$ animals ($n = 12$) were able to learn the task as well as their age-matched WT controls ($n = 10$): although the mean distance to locate the submerged platform on the last three days of training was longer in mutant mice compared to $CrT^{+/y}$ littermates (*t*-test, $P < 0.05$), they exhibited a progressive reduction of the path length similar to WT littermates (Two-Way RM ANOVA, $P = 0.084$ effect of genotype) with a significant difference between the two groups only at the day 5 of training (post hoc Holm-Sidak method, $P < 0.05$; Fig. 3A). The same was true in P100 animals ($CrT^{-/y}$: $n = 8$, $CrT^{+/y}$: $n = 7$; Two-way RM ANOVA on rank transformed data, $P = 0.132$ effect of genotype, post hoc Holm-Sidak method, $P < 0.05$ at day 5; Fig. 3B). In contrast, $CrT^{-/y}$ mice ($n = 7$) were significantly slower learners with respect to age-matched WT mice ($n = 9$) at P180 so much so that the distance to locate the platform was different between the two groups at days 3, 4, 5 and 6 of training (Two-Way RM ANOVA on rank transformed data, genotype, $P < 0.001$, interaction between genotype and day $P < 0.001$; post hoc Holm-Sidak method, $P < 0.05$ for day 3 and 6, $P < 0.01$ for day 4 and 5; Fig. 3C).

To further corroborate the hypothesis of a premature cognitive decline in CrT null mice, we compared the performance in the MWM of P180 $CrT^{-/y}$ animals and one-year old wild-type mice ($n = 4$). The mean distance to locate the platform on the last three days of training (*t*-test, $P = 0.968$; Supplementary Material, Fig. S5A) and the probe test revealed a similar learning and memory impairment in these two experimental groups (Two-Way RM ANOVA, $P = 0.479$; Supplementary Material, Fig. S5B).

Emotional phenotype is not altered in CrT mutant animals

To rule out the possibility that significant differences in cognitive capacities reflect changes in the ability to cope with stress in challenging task conditions, we analysed the general activity and anxiety-related behaviour of $CrT^{-/y}$ and $CrT^{+/y}$ mice in the open field arena at the different ages used for cognitive assessment. We found that the time spent by $CrT^{-/y}$ mutant mice ($n = 12$ for P40 and P100, $n = 11$ for P180) in both the central and peripheral portion of the apparatus was not different from that recorded for WT animals ($n = 13$ for P40 and P100, $n = 11$ for P180) at any of the time point tested (Two Way ANOVA, post hoc Holm-Sidak method, $P = 0.725$ (P40), $P = 0.508$ (P100) and $P = 0.348$ (P180)), indicating that the vulnerability to stress and anxiety responses are not sensitive to CrT deletion and excluding the hypothesis that the progression of cognitive deficit might be related to altered emotionality (Supplementary Material, Fig. S6).

$CrT^{-/y}$ mice exhibit increased repetitive and stereotyped behaviour

Since the clinical picture of CCDS1 patients includes multiple traits linked to autism spectrum disorders (ASDs), we also

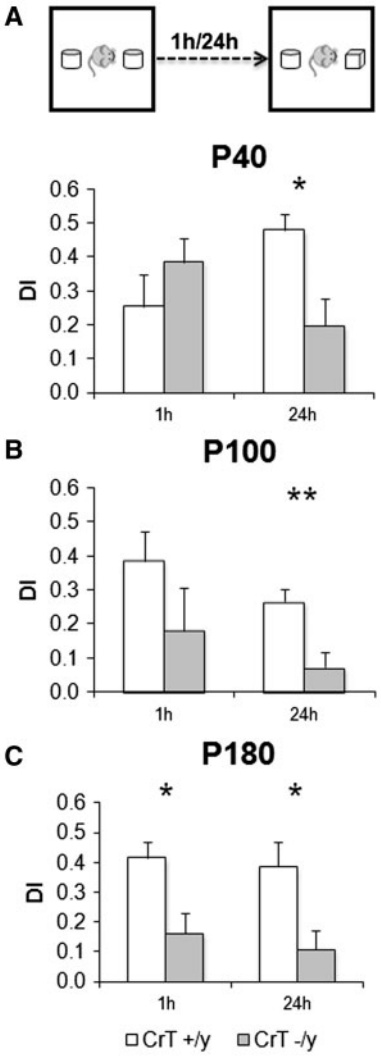

Figure 2. Progressive impairment of object recognition memory in CrT$^{-/y}$ mice. Top, a schematic representation of the object recognition task. Histograms display object discrimination indexes of CrT$^{+/y}$ and CrT$^{-/y}$ during the testing phase performed after a delay of 1 and 24h since the sample phase at different ages. (**A**) P40. While both experimental groups can recognize the new object in the test at 1h (*t*-test, $P = 0.285$), a significantly lower discrimination index was found in CrT$^{-/y}$ mice ($n = 9$) compared to CrT$^{+/y}$ animals ($n = 7$; *t*-test, $P < 0.05$). (**B**) P100. Even if still not significant, the recall capacity of CrT$^{-/y}$ animals at 1h was reduced (*t*-test, $P = 0.242$). At 24h, a *t*-test revealed that the performance of CrT$^{-/y}$ animals ($n = 11$) was strongly impaired with respect to controls ($n = 10$; $P < 0.01$). (**C**) P180. A significant deficit of both short (*t*-test, $P < 0.05$) and long-term (*t*-test, $P < 0.05$) memory was detected in mutant mice ($n = 10$) compared to controls ($n = 9$). *$P < 0.05$; **$P < 0.01$. Error bars, s.e.m.

examined social behaviour in CrT null mice. Although we used two different social interaction paradigms, we detected no abnormalities in CrT$^{-/y}$ mice at P180. In the social preference test, indeed, both CrT$^{-/y}$ ($n = 8$) and CrT$^{+/y}$ ($n = 6$) animals spent significantly more time exploring the wire cup housing the conspecific subject (Mann–Whitney Rank Sum test, $P = 0.662$; Fig. 4A). Similarly, the index measured in the social novelty task did not differ between mutant and WT mice (*t*-test, $P = 0.784$; Fig. 4A).

The second core ASD symptom domain includes repetitive and stereotyped movements, routines, and rituals (23) and several mouse lines with ASD-associated mutations exhibit enhanced learning on the accelerating rotarod, a task that requires formation and consolidation of a repetitive motor routine (24). Thus, we tested rotarod abilities of CrT$^{-/y}$ ($n = 12$ for P40, $n = 11$ for P100 and $n = 9$ for P180) and CrT$^{+/y}$ ($n = 13$ for P40 and P100, $n = 11$ for P180) animals, with the speed of rotation accelerating from 4 to 40 rpm over 600 s. The performance of CrT$^{-/y}$ mutant mice diverged from that of wild-type mice, with a significant increase of fall latency from the drum at all ages tested (Two Way ANOVA, effect of genotype $P < 0.001$, post hoc Holm Sidak method, $P < 0.01$ at P40 and P100, $P < 0.05$ at P180; Fig. 4B). We next examined self-grooming, another stereotyped behaviour in mice (25). While no difference was present at P40 (CrT$^{-/y}$, $n = 9$; CrT$^{+/y}$, $n = 7$; Two Way ANOVA on rank transformed data, post hoc Holm Sidak method, $P = 0.912$) CrT null mice spent about threefold as much time grooming themselves as littermate WT mice at P180 (CrT$^{-/y}$, $n = 7$; CrT$^{+/y}$, $n = 11$; $P < 0.01$; Fig. 4C).

CrT deletion leads to a widespread Cr reduction in young and adult mice

To understand whether the progression of cognitive deficits in CrT$^{-/y}$ mice was due to a gradual reduction of brain Cr content, we measured Cr levels in various tissues in 1-month- and 6-month-old animals using GC/MS. At both ages, we observed a significant reduction of Cr in the brain (both cerebral cortex and hippocampus; Two Way ANOVA on rank transformed data, post hoc Holm-Sidak method, $P < 0.001$), muscle ($P < 0.001$), heart ($P < 0.001$) and kidney ($P < 0.05$) of CrT$^{-/y}$ mice with respect to wild-type littermates ($n = 4$/tissue for each group; Table 1). Importantly, no difference was detected in Cr levels measured in the different tissues between P30 and P180 CrT$^{-/y}$ mice, except for the muscle: a Three way ANOVA on rank transformed data analysis revealed a significant interaction ($P < 0.001$) between genotype and age only at level of muscular tissue with a significant reduction of Cr levels in P180 CrT$^{-/y}$ mice (post hoc Holm-Sidak method, $P < 0.001$). A moderate change in GAA levels was observed in some tissues (Table 2) suggesting that Cr deficiency leads to a compensatory attempt by upregulating Cr biosynthesis. Also in this case GAA content measured in P180 animals reproduced the levels reported in younger tissues: a Three way ANOVA on rank transformed data revealed a significant interaction ($P < 0.001$) between genotype and age only at level of muscular tissue, but this analysis only stressed a significant reduction of GAA levels in P180 CrT$^{-/y}$ (post hoc Holm-Sidak method, $P < 0.05$) and WT mice ($P < 0.001$). These results allow rejecting the hypothesis that higher GAA toxicity could underlie the age-related decline of cognitive functions in CrT$^{-/y}$ animals.

Morphological characterization of neural circuits in CrT$^{-/y}$ mice

The morpho-functional organization of neural circuits in mice carrying CrT mutations has never been studied so far. Thus, we have investigated whether the accelerated decline of learning and memory functions in CrT-deficient mice was accompanied by pathological changes in brain morphology. The cerebral cortex and the hippocampus were analysed because they are strictly involved with the symptoms caused by CrT deficiency in mice and in humans. In the same animals subjected to behavioural characterization, we first evaluated the neuroanatomical architecture of prefrontal (PFC) and cingulate cortex (ACC) of

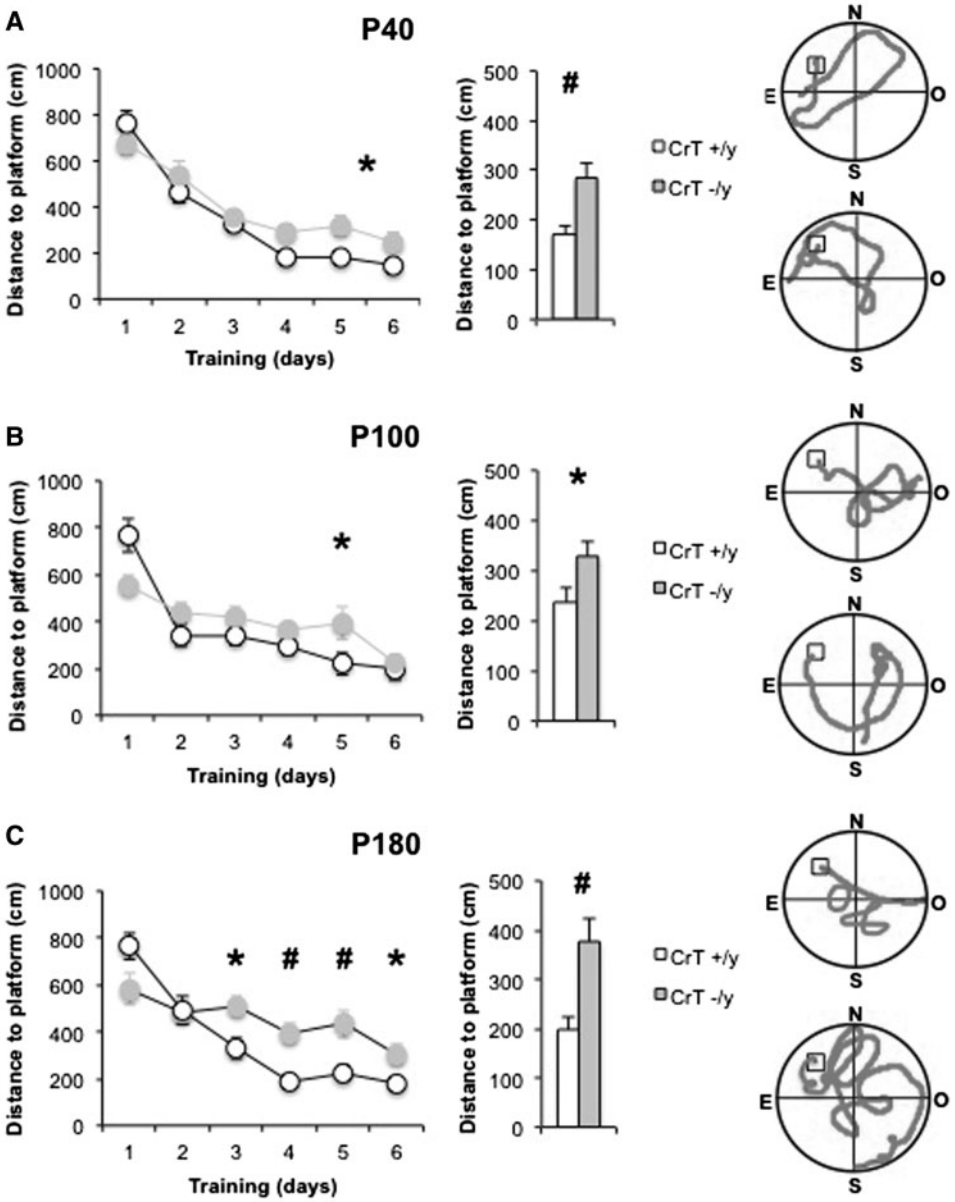

Figure 3. CrT deletion progressively deteriorates spatial learning and memory in mutant mice. (**A**) Left, learning curves for $CrT^{+/y}$ ($n = 10$, white) and $CrT^{-/y}$ mice ($n = 12$, grey) at P40. A significant difference was detected at day 5 (Two way RM ANOVA, post hoc Holm-Sidak method, $P < 0.05$). Right, histograms showing the mean swimming path covered to locate the submerged platform on the last three days of training for the two groups. A significant difference between $CrT^{-/y}$ and $CrT^{+/y}$ animals was present (*t*-test, $P < 0.01$). Representative examples of swimming path during the day 3 of the training phase for a $CrT^{+/y}$ (top) and a $CrT^{-/y}$ mouse (bottom) are also reported. (**B**) Left, learning curves for $CrT^{+/y}$ ($n = 7$, white) and $CrT^{-/y}$ mice ($n = 8$, grey) at P100. A significant difference was detected at day 5 (Two way RM ANOVA, post hoc Holm-Sidak method, $P < 0.05$). Right, histograms showing the mean swimming path on the last three training days for the two groups. A significant difference between $CrT^{+/y}$ and $CrT^{-/y}$ animals was present (*t*-test, $P < 0.05$). Representative examples of swimming path during the day 3 of the training phase for a $CrT^{+/y}$ (top) and a $CrT^{-/y}$ mouse (bottom) are also reported. (**C**) Left, learning curves for $CrT^{+/y}$ ($n = 9$, white) and $CrT^{-/y}$ mice ($n = 7$, grey) at P180: mutant mice were poorer learners with respect to control littermates and a significant difference was detected at day 3, 4, 5 and 6 (Two way RM ANOVA on rank transformed data, post hoc Holm-Sidak method, $P < 0.05$ for day 3 and 6, $P < 0.01$ for day 4 and 5). Right, histograms showing the mean swimming path on the last three day of training. A *t*-test analysis showed a statistical difference between $CrT^{+/y}$ and $CrT^{-/y}$ animals ($P < 0.01$). Representative examples of swimming path during the day 3 of the training phase for a $CrT^{+/y}$ (top) and a $CrT^{-/y}$ mouse (bottom) are also depicted. $^{*}P < 0.05$; $^{\#}P < 0.01$. Error bars, s.e.m.

P180 mice ($n = 6$ for both groups). Cortical thickness and neuronal cell density was estimated on NeuN stained sections. No difference in the cortical thickness (*t*-test, $P = 0.785$ for PFC and $P = 0.880$ for ACC; Supplementary Material, Fig. S6) and neuronal density across cortical layers was observed in mutant animals (Two Way ANOVA, $P = 0.683$ for PFC; Two Way ANOVA on rank transformed data, $P = 0.146$ for ACC; Supplementary Material, Fig. S7).

Loss of GABAergic synapses in the cerebral cortex of $CrT^{-/y}$ mice

Since synaptic dysfunction is a feature commonly observed in normal aging and neurodegenerative disorders likely contributing to the pathology progression (26), we analysed the synaptic punctate expression of vGlut1 and vGAT, respectively as synaptic markers of excitatory and inhibitory neurons, in the cerebral

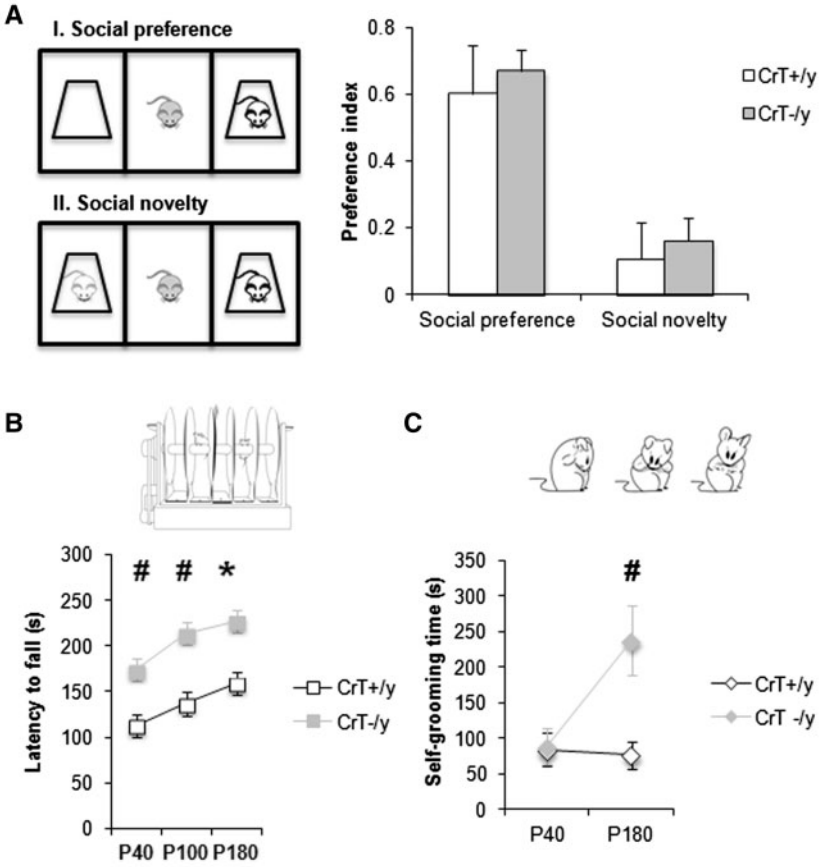

Figure 4. CrT mutation enhances repetitive and stereotyped behaviours. (**A**) Social interaction behaviours in $CrT^{-/y}$ mice. Histograms display discrimination indexes of $CrT^{+/y}$ ($n = 6$) and $CrT^{-/y}$ ($n = 8$) mice during the social preference (session I) and the social novelty phase (session II). No difference was detected between the two groups (Mann–Whitney Rank Sum test, $P = 0.662$ for session I; *t*-test, $P = 0.784$ for session II). A schematic representation of the three-chamber test is also depicted. (**B**) Performance of littermate wild-type ($n = 11$) and $CrT^{-/y}$ mice ($n = 9$) on the accelerating rotarod. Inset shows an illustration of the rotarod apparatus. A two-way ANOVA showed a significant effect of genotype ($P < 0.001$). Post hoc Holm-Sidak test revealed that the fall latency of mutant animals was significantly different from that of wild-type mice at all ages tested ($P < 0.01$ at P40 and P100, $P < 0.05$ at P180). (**C**) Histograms display mean time spent self-grooming in $CrT^{+/y}$ and $CrT^{-/y}$ animals at P40 and P180. While no difference was detected at P40 ($CrT^{+/y}$, $n = 7$; $CrT^{-/y}$, $n = 9$; Two Way ANOVA on rank transformed data, post hoc Holm Sidak method, $P = 0.912$), CrT null mice exhibit increased grooming behaviour at P180 ($CrT^{+/y}$, $n = 11$; $CrT^{-/y}$, $n = 7$; $P < 0.01$). A schematic representation of self-grooming behaviour is reported.*$P < 0.05$; #$P < 0.01$. Error bars, s.e.m.

Table 1 Cr levels (mean ± s.e.m.) in $CrT^{+/y}$ and $CrT^{-/y}$ animals at P30 and P180 ($n = 4$ per tissue for both groups). Cr levels have been measured by GC/MS. A reduction of Cr content was evident in the brain, muscle, heart and kidney of mutant animals at both P30 and P180 (Two Way ANOVA on rank transformed data, post hoc Holm-Sidak method). *$P < 0.05$; **$P < 0.01$; ***$P < 0.001$

Tissue (nmol/mg protein)	P30		P180	
	$CrT^{+/y}$	$CrT^{-/y}$	$CrT^{+/y}$	$CrT^{-/y}$
Cortex	76.36 ± 3.16	13.61 ± 1.06***	92.41 ± 0.66	14.15 ± 0.66***
Hippocampus	83.69 ± 4.37	14.14 ± 1.52***	88.73 ± 4.97	14.79 ± 1.46***
Muscle	310.20 ± 31.59	111.57 ± 21.27***	365.38 ± 8.19	15.94 ± 5.55***
Heart	89.92 ± 5.15	1.19 ± 0.27***	100.91 ± 3.36	2.39 ± 0.61***
Kidney	9.60 ± 0.65	1.59 ± 0.13*	10.36 ± 0.80	1.80 ± 0.78**

cortex of $CrT^{-/y}$ mice. While excitatory synapses were not affected by Cr deficiency ($n = 6$ for both groups; Mann–Whitney Rank Sum test, $P = 0.792$ for PFC; *t*-test, $P = 0.340$ for ACC; Fig. 5A), we detected a prominent loss of vGAT staining both in PFC and ACC, suggesting a specific contribution of GABAergic

Table 2 GAA levels (mean ± s.e.m.) in $CrT^{+/y}$ and $CrT^{-/y}$ animals at P30 and P180 ($n = 4$ per tissue for both groups). At P30, a moderate increase of GAA content was evident in the brain and the muscle of mutant animals (Two Way ANOVA on rank transformed data, post hoc Holm-Sidak method, $P < 0.05$), whereas GAA was decreased in the heart of $CrT^{-/y}$ animals ($P < 0.05$) and no difference was detected in the kidney tissue ($P = 0.359$). At P180, GAA levels were higher in the hippocampus and the muscle of mutant animals (Two-way ANOVA on rank transformed data, post hoc Holm-Sidak method, $P < 0.01$), whereas no difference was detected in cortex, heart and kidney ($P = 0.175$, $P = 0.320$ and $P = 0.920$, respectively). **$P < 0.01$; ***$P < 0.001$

Tissue (nmol/mg protein)	P30		P180	
	$CrT^{+/y}$	$CrT^{-/y}$	$CrT^{+/y}$	$CrT^{-/y}$
Cortex	0.060 ± 0.002	0.114 ± 0.016***	0.050 ± 0.006	0.066 ± 0.005
Hippocampus	0	0.091 ± 0.007 ***	0.026 ± 0.015	0.079 ± 0.009**
Muscle	0.106 ± 0.006	0.282 ± 0.068**	0.026 ± 0.010	0.150 ± 0.050**
Heart	0.094 ± 0.010	0.060 ± 0.004***	0.052 ± 0.007	0.033 ± 0.015
Kidney	10.700 ± 0.627	9.758 ± 0.712	2.205 ± 0.259	2. 411 ± 0.112

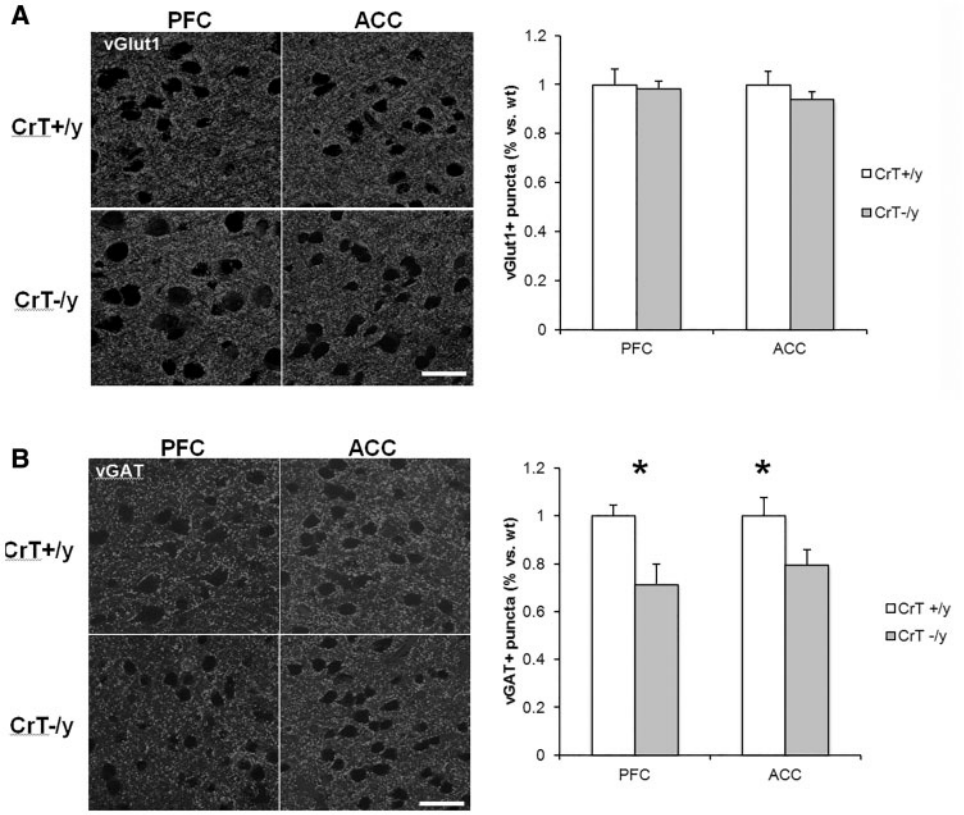

Figure 5. Synaptic neurotransmission in $CrT^{+/y}$ and $CrT^{-/y}$ animals at P180. (**A**) Left, representative immunostaining for vGlut1 from PFC and ACC of a $CrT^{+/y}$ and a $CrT^{-/y}$ mouse. Right, no difference in vGlut1 staining was detected between the two experimental groups ($n = 6$ for both groups) either in PFC (t-test, $P = 0.792$) or ACC (t-test, $P = 0.340$). (**B**) Left, representative immunostaining for vGAT from PFC and ACC of a $CrT^{+/y}$ and a $CrT^{-/y}$ mouse. The number of vGAT-positive puncta was significantly reduced both in the PFC and the ACC of mutant animals ($n = 9$) with respect to controls ($n = 8$; t-test, $P < 0.05$ for both comparisons). *$P < 0.05$. Calibration bars: 25 μm. Error bars, s.e.m.

synaptic alterations to the neuropathological phenotype of CCDS1 ($n = 9$ for $CrT^{-/y}$ group, $n = 8$ $CrT^{+/y}$ group; t-test, $P < 0.05$ for both comparisons; Fig. 5B). Importantly, the loss of vGAT-positive synapses overspread all the cortical layers. These results are also consistent with previous studies on CCDS1 patients exhibiting evidence for an epileptic phenotype (27) that could be predictive of a dysfunction of inhibitory interneurons.

Microglial cell dysregulation in Cr deficient brain

Since aberrant microglia activation is one of the main pathological hallmarks of brain aging (28,29), we have also evaluated Iba-1 expression as a marker of possible morphological changes of microglia in the cerebral cortex (PFC) and the hippocampus (HP) of mutant mice. During aging microglia cells undergo morphological changes towards a reactive phenotype with short, thickened and less ramified processes (30). We found a strong increase of activated microglial cells in the brain of CrT null animals as compared to wild-type controls ($n = 8$ for both groups), with a parallel reduction of resting cells (Two Way ANOVA, post hoc Holm Sidak method, $P < 0.01$ for PFC and $P < 0.05$ for HP; Fig. 6A and B), indicating that the metabolic deficit caused by Cr deficiency leads to a dysfunction of brain-immune cells interactions and to a neuroinflammatory state that can contribute to the cognitive decline reported in $CrT^{-/y}$ mice.

Reduced neurogenesis and enhanced lipofuscin accumulation in the hippocampus of $CrT^{-/y}$ mice

It is well-known that the rate of neurogenesis declines dramatically with age and dysregulation of hippocampal neurogenesis is an important mechanism underlying the cognitive impairment associated with normal aging (31). In order to investigate whether CrT deficiency could affect hippocampal structure and impinge on the neurogenesis process, we examined neuronal proliferation through Ki67 labelling in the dentate gyrus (DG) of wild type and $CrT^{-/y}$ mice ($n = 6$ for both groups). Stereological analysis first revealed that the hippocampal volume of mutant animals was markedly reduced with respect to that measured in control mice (t-test, $P < 0.05$; Fig. 7A). The number of Ki67-positive cell was significantly lower in the DG of $CrT^{-/y}$ animal at P180, with approximately 30% reduction (t-test, $P < 0.01$; Fig. 7B and D). We also evaluated the number of immature neurons in hippocampal DG using the neuroblast marker doublecortin (DCX). DCX-positive cells were also significantly reduced in CrT null mice DG (t-test, $P < 0.001$; Fig. 7C and E), demonstrating the impairment of adult hippocampal neurogenesis and suggesting another

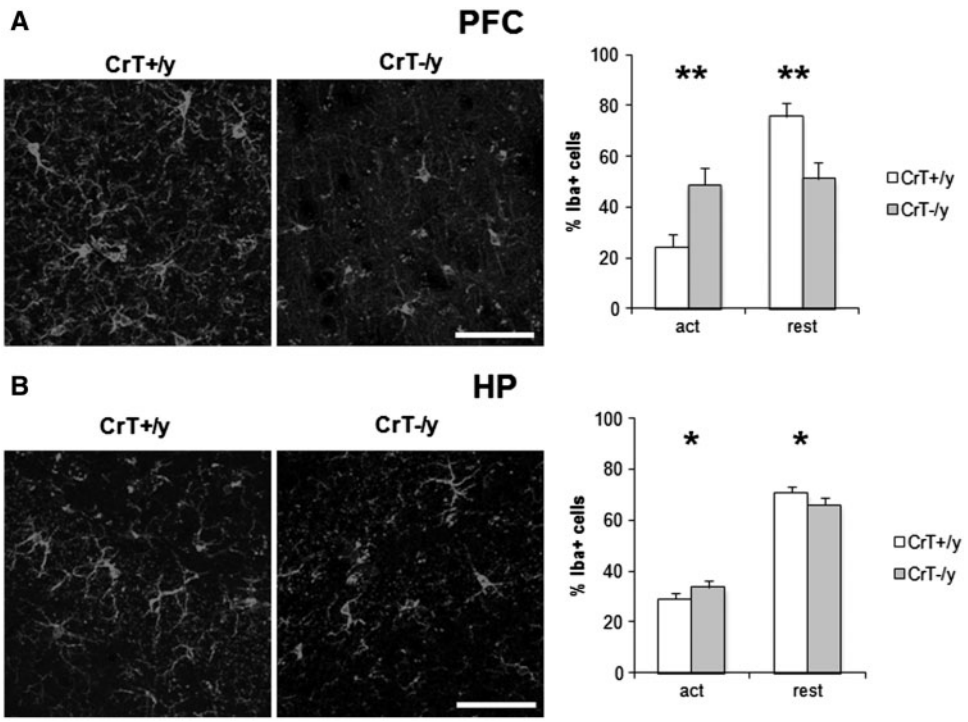

Figure 6. Pathological activation of microglial cells in $CrT^{-/y}$ animals (A) Left, representative immunostaining for Iba-1 from prefrontal cortex (PFC) of a $CrT^{+/y}$ and a $CrT^{-/y}$ mouse. Right, a significant increase of the percentage of activated microglial cells, with a parallel decrease of resting microglia, was detected in mutant mice with respect to wild-type animals ($n = 8$ for both groups; Two Way ANOVA, post hoc Holm Sidak method, $P < 0.01$). (B) Left, representative immunostaining for Iba-1 from the hippocampus (HP) of a $CrT^{+/y}$ and a $CrT^{-/y}$ mouse. Right, the percentage of activated microglia was increased in mutant mice, whereas the relative number of resting cells was reduced compared to controls ($n = 8$ for both groups; Two Way ANOVA, post hoc Holm Sidak method, $P < 0.05$). *$P < 0.05$; **$P < 0.01$. Calibration bar: 100 μm. Error bars, s.e.m.

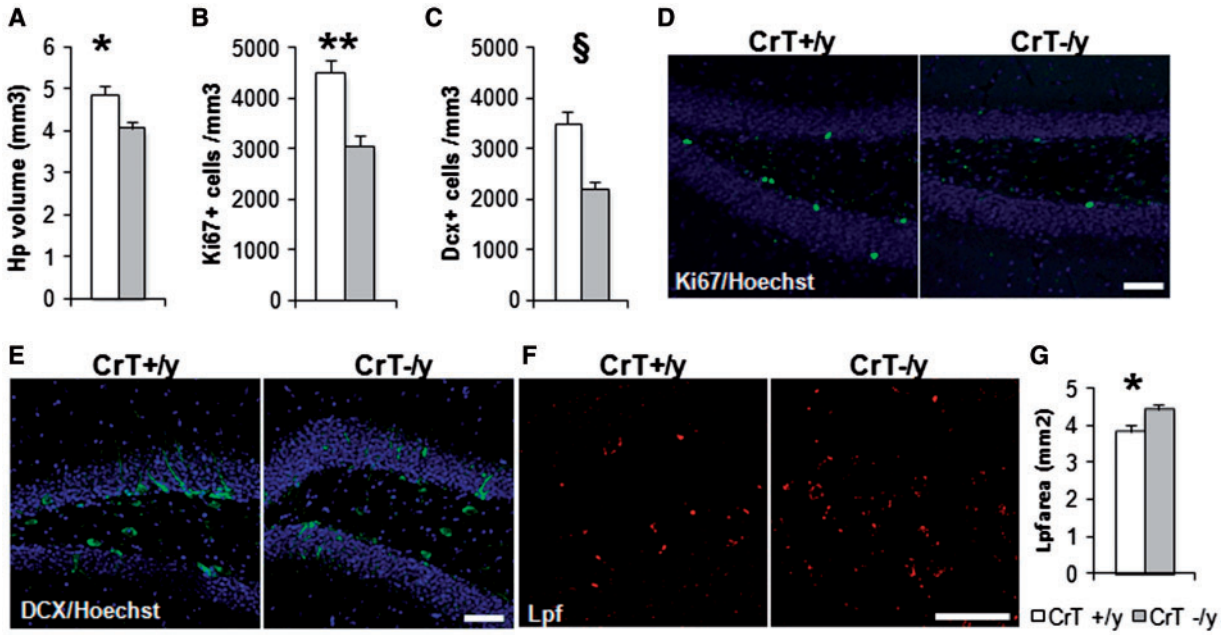

Figure 7. Neurogenesis impairment and enhanced lipofuscin accumulation in the hippocampus of $CrT^{-/y}$ animals at P180. (A) The hippocampal volume of $CrT^{-/y}$ mice was smaller compared to $CrT^{+/y}$ mice ($n = 6$ for both groups; t-test, $P < 0.05$). (B) Stereological counting revealed that the density of Ki67-positive cells was significantly reduced in the DG of $CrT^{-/y}$ mice, with approximately 30% reduction with respect to wild-type littermates ($n = 6$ for both groups; t-test, $P < 0.01$). (C) A significant decrease of the DCX-positive immature neurons was detected in the hippocampus of adult $CrT^{-/y}$ mice compared to controls ($n = 6$ for both groups; t-test, $P < 0.001$). (D) Representative immunostaining for Ki-67, a nuclear protein required for cellular proliferation, from a $CrT^{+/y}$ and a $CrT^{-/y}$ mouse. (E) Representative immunostaining for DCX, a microtubule-associated phosphoprotein expressed in early neuronal differentiation, from a $CrT^{+/y}$ and a $CrT^{-/y}$ mouse. (F) Representative images for lipofuscin autofluorescence from a $CrT^{+/y}$ and a $CrT^{-/y}$ mouse. (G) Six-month-old $CrT^{-/y}$ mice ($n = 6$) show extensive accumulation of autofluorescent material throughout the brain when compared to the wild-type control ($n = 5$). A significant increase of abnormal autofluorescent storage was mainly found in DG granular and polymorph layer of $CrT^{-/y}$ mice (t-test, $P < 0.05$). *$P < 0.05$; **$P < 0.01$; §$P < 0.001$. Calibration bars: 50 μm. Error bars, s.e.m.

cellular substrate of the cognitive deficit present in the CrT null model.

Another characteristic neuropathological finding in CrT mice was the massive accumulation of autofluorescent material (lipofuscin). Lipofuscin is a lipopigment consisting of aggregated products of lysosomal degradation, including oxidized and misfolded proteins, lipids, defective mitochondria and metal ions (32). We observed a marked accumulation of autofluorescent lipofuscin throughout the brain, but the most prominent autofluorescent signal was seen in the DG hippocampal region. Lipofuscin deposition and accumulation within the hippocampal neurons is a marker of cellular senescence (33,34). Thus, we compared the area of lipofuscin granules in the brain cells of 6-month-old $CrT^{-/y}$ ($n=6$) mice and their $CrT^{+/y}$ siblings ($n=5$). The accumulation of lipofuscin was significantly exacerbated in the hippocampal DG of $CrT^{-/y}$ animals at P180 (*t*-test, $P<0.05$, Fig. 7F and G).

A conditional brain-specific model of CCDS1 recapitulates the phenotype displayed by $CrT^{-/y}$ mice

Since $CrT^{-/y}$ mice with ubiquitous deletion of the CrT gene showed a marked Cr depletion also in peripheral tissues, we analysed a novel mouse model in which a conditional CrT allele was deleted in postmitotic neurons, glial cells and BBB endothelial cells by using the Nestin promoter to drive Cre-recombinase expression (35; nes-CrT mice).

As expected, biochemical analysis in these mice highlighted a depletion of Cr (and a parallel increase of GAA), similar to that of the null CrT mouse, but totally restricted to the brain tissue, with peripheral tissues being not affected (Tables 3 and 4). Importantly, we also observed that $CrT^{fl/y}$ animals not expressing Cre recombinase did not present a hypomorph phenotype, with normal levels of Cr in different tissues (Tables 3 and 4). Behavioural investigation highlighted that mutant (nes-$CrT^{-/y}$) animals showed an impaired performance in the object recognition test (Fig. 8A) and a lower alternation rate in the Y maze (Fig. 8B), demonstrating an impairment of both declarative and working memory reminiscent of the deficit described in the ubiquitary model. More specifically, at P180 nes-$CrT^{-/y}$ mice displayed an impaired discrimination index with respect to nes-$CrT^{+/y}$ mice both at 1- and 24-h interval between the sample and the test phase (nes-$CrT^{-/y}$ $n=6$, nes- $CrT^{+/y}$ $n=8$; *t*-test, $P<0.05$ for both comparisons; Fig. 8A). In the Y maze, the alternation rate of nes-$CrT^{-/y}$ mice ($n=6$) was about 10% lower of that reported for nes-$CrT^{+/y}$ animals ($n=6$; *t*-test, $P<0.05$; Fig. 8B). We also investigated whether the selective CrT deficiency could affect hippocampal neurogenesis. Stereological analysis revealed that the number of Ki67-positive cell was significantly lower in the DG of nes-$CrT^{-/y}$ animal at P180 compared to age-matched controls ($n=6$ for both group; *t*-test, $P<0.05$; Fig. 8C). These results prove that the lack of CrT protein exclusively restricted to brain cells is sufficient to recapitulate the cognitive and cellular defects displayed by global knock-out mice.

Table 3 Cr levels (mean ± s.e.m.) in nes-$CrT^{+/y}$, nes-$CrT^{-/y}$ and $CrT^{fl/y}$ animals at P180 ($n=4$ per tissue for all groups). A reduction of Cr content was evident in the brain of mutant animals, while peripheral tissues were not affected (Two-way ANOVA on rank transformed data, post hoc Holm-Sidak method). ***$P<0.001$

Tissue (nmol/mg protein)	nes-$CrT^{+/y}$	nes-$CrT^{-/y}$	$CrT^{fl/y}$
Cortex	73.29 ± 1.88	17.36 ± 0.87***	71.55 ± 4.15
Hippocampus	87.45 ± 4.17	17.13 ± 2.22***	94.62 ± 4.35
Muscle	382.97 ± 20.46	390.58 ± 22.66	385.36 ± 27.59
Heart	78.24 ± 3.72	70.35 ± 3.10	68.02 ± 1.79
Kidney	6.10 ± 0.81	3.11 ± 0.27	7.60 ± 1.22

Table 4 GAA levels (mean ± s.e.m.) in nes-$CrT^{+/y}$, nes-$CrT^{-/y}$ and $CrT^{fl/y}$ animals at P180 ($n=4$ per tissue for all groups). An increase of GAA content was evident in the brain of mutant animals, while peripheral tissues were not affected (Two-way ANOVA on rank transformed data, post hoc Holm-Sidak method). *$P<0.05$; ***$P<0.001$

Tissue (nmol/mg protein)	nes-$CrT^{+/y}$	nes-$CrT^{-/y}$	$CrT^{fl/y}$
Cortex	0.048 ± 0.005	0.059 ± 0.004***	0.048 ± 0.004
Hippocampus	0.068 ± 0.005	0.131 ± 0.018*	0.074 ± 0.011
Muscle	0.054 ± 0.006	0.061 ± 0.002	0.059 ± 0.003
Heart	0.045 ± 0.004	0.047 ± 0.003	0.054 ± 0.007
Kidney	1.705 ± 0.373	1.231 ± 0.099	3.051 ± 0.914

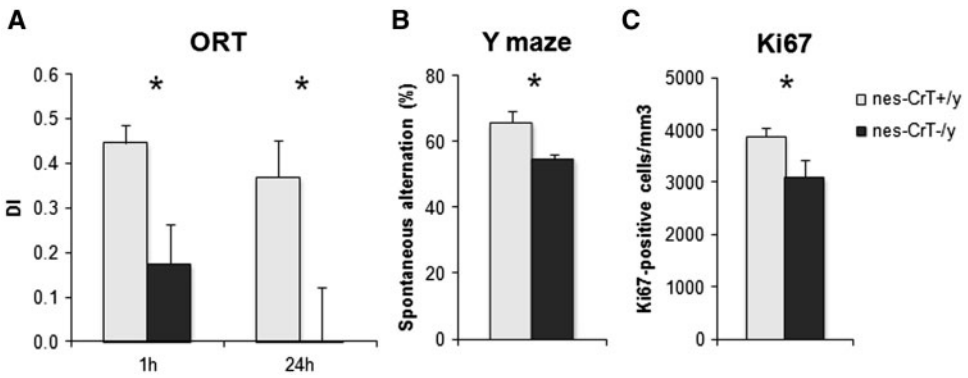

Figure 8. A selective brain deletion of CrT is sufficient to impair cognitive functions and hippocampal neurogenesis. (**A**) Histograms display object discrimination indexes of nes-$CrT^{+/y}$ and nes-$CrT^{-/y}$ during the testing phase performed after a delay of 1 and 24h since the sample phase at P180. A significant deficit of both short- (*t*-test, $P<0.05$) and long-term (*t*-test, $P<0.05$) memory was detected in mutant mice ($n=6$) compared to controls ($n=8$). (**B**) Alternation rate in the Y maze was significantly lower in nes-$CrT^{-/y}$ mice ($n=6$) compared to that recorded for nes-$CrT^{+/y}$ littermates ($n=9$; t test, $P<0.05$) at P180. (**C**) A significant decrease of the Ki67-positive cells was detected in the hippocampus of P180 nes-$CrT^{-/y}$ mice compared to age-matched controls ($n=6$ for both groups; *t*-test, $P<0.05$). *$P<0.05$. Error bars, s.e.m.

Discussion

CCDS1 is known to cause brain Cr depletion and several neurological deficits, but nothing is known about the neurobiological basis of this disease. We performed the first analysis of morphological, cellular and behavioural impairments in a CCDS1 mouse model. The results report the earliest cognitive phenotype observed so far in CCDS1 mice, and a novel behavioural phenotype consisting in enhanced stereotypies. Moreover, we found that phenotypes associated with brain aging, including a progressive learning and memory deterioration, synaptic loss, microglial cell activation, neurogenesis impairment and lipofuscin deposition already occur in adult animals. The significant differences in learning and memory performance of $CrT^{-/y}$ mice reflected changes in cognitive abilities *per se*: indeed, the open field test revealed that mutant mice display anxiety levels in the range of normal values, indicating that their capacity to cope with stressful conditions of behavioural tests is not altered.

It is essential noticing that the main organ affected in human CCDS1 is the brain, with patients showing normal cardiac function and unaltered Cr levels in the muscle (2). In contrast, $CrT^{-/y}$ mice displayed a marked reduction of Cr also in peripheral tissues. To understand whether the cognitive phenotype observed in CrT null mice depends on the brain CrT deletion or if peripheral factors may also play a key role, we analysed learning and memory in a mouse model in which CrT deletion was restricted to the brain. Our results demonstrate that Cr brain-specific depletion is sufficient to cause a cognitive impairment indistinguishable from that of mice with ubiquitous CrT deletion.

The role of Cr deficiency in aging process: novel mechanistic insights

An important question raised by the premature aging of $CrT^{-/y}$ mice concerns the role of Cr deficiency in the aging process. It is worth noting that the cognitive regression of $CrT^{-/y}$ animals was not paralleled by either a decrease of Cr levels in the brain tissue or a rise of GAA toxicity, suggesting that the prolonged lack of Cr energy buffer may set in motion cellular compensatory mechanisms leading to the gradual shutdown of brain function. We detected a significant reduction of Cr levels in P180 $CrT^{-/y}$ mice with respect to P30 CrT null mice only at level of muscular tissue, indicating that compensatory upregulation of Cr in the muscle declines with age. Despite the ubiquitary pattern of CrT deletion, only few CCDS1 patients displayed an alteration of muscular Cr levels and strength (36). Our results raise the possibility that a muscular phenotype could occur also in patients later in life.

We have considered the possibility that the accelerated decline in cognitive performance in mature $CrT^{-/y}$ animals could be related to the documented neuroprotective (15,36,37,38) and anti-apoptotic effects of Cr (39). However, when we examined the neuronal density in the cerebral cortex, we did not detect any significant reduction in the number of NeuN-positive cells either in the PFC or in the ACC. In contrast, we found a marked impairment of hippocampal neurogenesis in the brain of mature $CrT^{-/y}$ mice. This was assessed by observing significantly reduced numbers of Ki67-positive proliferating cells along with DCX-positive immature neurons in the hippocampal DG region. These results are consistent with the notion that the creation of new neurons is an energetically expensive process (40) and that the hippocampus is particularly vulnerable to metabolic alterations (41). Since adult hippocampal neurogenesis plays a vital role in maintaining normal cognitive processing (41,42), an impairment of this process could conceivably compromise hippocampal function and represent a key substrate of the cognitive defects seen in $CrT^{-/y}$ mice. Accordingly, most studies indicate a correlation between a compromised neurogenic niche and impaired performance in hippocampus-dependent cognitive tasks in aged mice (31).

In addition, we observed that long-term Cr deficiency induce a more subtle and specific reorganization of neuronal circuits consisting in significantly lower expression of the vesicular GABA transporter. This alteration, which has been detected in two brain regions fundamentally involved in the processing of learning and memory tasks such as the PFC and the ACC, could be mirrored by a significant dysfunction of synaptic activity leading to increased cognitive frailty. It has been reported, indeed, that alterations in inhibitory interneurons contribute to cognitive deficits associated with aging and neurological diseases (43,44).

One of the principal findings of this work is the demonstration that neuroinflammation plays a critical role in the progression of CrT disorder. It is apparent that Cr deficiency causes an aberrant activation of microglial cells in the brain of mature $CrT^{-/y}$ animals and activated microglia may release a number of cytokines and chemokines, which in turn activate many proinflammatory signal transduction pathways. It is known that co-activation of proinflammatory and cytotoxic products during neuroinflammation process is detrimental to neurons and may alter synaptic proteins (45). Several studies, indeed, showed a significant downregulation of protein and mRNA levels of synaptic markers in animal models of neuroinflammation such as a non-infectious rat model of HIV-1 and rats treated with a high dose of lipopolysaccharide (46,47). Recent evidence demonstrates that neuroinflammation also negatively affects hippocampal neurogenesis (48,49). We could hypothesize that activated microglia-neuron crosstalk has detrimental effects on hippocampal neurogenesis and brain synaptic connectivity in $CrT^{-/y}$ animals. Thus, the dysregulation of microglial behaviour appears to be a critical component of the negative progression of CrT deficiency pathology.

A possible trigger of neuroinflammation is the increased concentration of damaged macromolecules and protein aggregates as a result of an increase in oxidative stress as well as of mitochondrial dysfunction leading to excessive generation of reactive oxygen species (ROS) and oxidative damage to lipids, proteins and DNA. The Cr/PCr system is strongly implicated in the cellular bioenergetic function and several studies have revealed a correlation between Cr levels and intracellular ROS inasmuch Cr exhibits antioxidant activity through either direct interaction with oxidant species or metabolic action conferring antioxidant protection (16,17). Accordingly, we found an enhanced accumulation of lipofuscin in the brain of $CrT^{-/y}$ mice that could be the result of increased oxidative damage (50). The presence of lipofuscin can also influence important cellular processes, such as autophagy, by inhibiting the fusion between autophagosomes and lysosomes, thus further exacerbating the accumulation of degradation products and cognitive impairment (51).

Since our morphological analysis of mutant brain was all performed in adult animals, future studies will need to check the developmental profile of marker modifications to better dissect cellular defects underlying the onset and progression of the pathological behavioural phenotype in CrT null mice.

Impact on CCDS1 patients

Present results have demonstrated that CrT null mice undergo to an early onset of brain aging. One fundamental conclusion

emerging from this work is that CCDS1 is a metabolic disorder associated with early brain aging and that age should be a key factor to deal with in the clinical evaluation of patients. It has been previously reported that patient intellectual disability becomes more pronounced with age (6), but longitudinal studies in patients are totally lacking and little is known about the progression of the disease.

In addition, our CrT mouse model allowed us to discover alterations of cellular and molecular mechanisms that play a pivotal role in the generation of the CCDS1 neurological phenotype. Mutant mice displayed alteration of GABAergic system, reduction of hippocampal neurogenesis, marked activation of microglia, and altered oxidative metabolism, leading to a general cognitive deterioration progressively worsening with age. This knowledge opens the important possibility to design targeted-drug intervention protocols aimed at overcoming brain alterations. If we could rescue brain alterations underlying CCDS1, indeed, both clinical and behavioural amelioration should be achieved. The use of non-invasive methods for behavioural assessment suitable for longitudinal analysis and the morphological characterization of brain alterations in $CrT^{-/y}$ mice set a firm background for translational studies using this model, providing normative data and protocols necessary to validate potential treatment strategies prior to launching costly clinical trials. Finally, our data also suggest that $CrT^{-/y}$ animals may serve as a useful model for exploring the mechanisms of age-related damage in the brain. A large number of neurodevelopmental and neurological disorders, including Down syndrome, Batten disease, progranulin deficiency, brain iron dysregulation, have been associated with early brain aging (52–55). Thus, a better understanding of factors that accelerate age-related deterioration of cognitive performance is critical both for improving the likelihood for successful aging and for revealing pathological changes of translational value.

Materials and Methods

Animals

As CrT deficiency is an X-linked pathology, male mice were selected for this study. $CrT^{-/y}$ and $CrT^{+/y}$ mice on a C57BL/6 J background were generated as described previously (11). Animals were maintained at 22 °C under a 12-h light–dark cycle (average illumination levels of 1.2 cd/m^2). Food (4RF25 GLP Certificate, Mucedola) and water were available *ad libitum*. To target CrT deletion to neuronal and glial cells of the central nervous system we used a mouse (35) expressing Cre recombinase under the Nestin promoter (Nestin:Cre). $CrT^{+/fl}$ females were crossed with Nestin:Cre male mice to generate a mouse line carrying the floxed CrT and Nestin:Cre alleles. Mice with three genotypes were used as experimental animals: mice carrying the brain specific deletion of CrT (Nestin:Cre-$CrT^{-/y}$, nes-$CrT^{-/y}$), mice expressing the floxed allele but not Cre-recombinase ($CrT^{fl/y}$), and mice expressing Cre-recombinase but not carrying the floxed allele (Nestin:Cre-$CrT^{+/y}$, nes-$CrT^{+/y}$). These genotypes were obtained in the same litters. Since $CrT^{fl/y}$ mice did not display any difference in Cr levels with respect to nes-$CrT^{+/y}$ animals, we performed behavioural and anatomical investigation only in the other two experimental groups. All experiments were carried out in accordance with the European Communities Council Directive of 24 November 1986 (86/609/EEC) and were approved by the Italian Ministry of Health (authorization number 259/2016-PR).

Detection of *Slc6a8* mutation by PCR

Genomic DNA was isolated from mouse tail using a kit, and the protocol suggested by the manufacturer (DNeasy Blood & Tissue Kit, Qiagen, USA). DNA was amplified for CrT mutant and wild-type alleles using a standard PCR protocol with the following primers: F:AGGTTTCCTCAGGTTATAGAGA; R:CCCTAGGT GTATCTAACATCT; R1: TCGTGGTATCGTTATGCGCC. Primers for Cre recombinase expression were: F: AACGCACTGATTTCGACC; R: CAACACCATTTTTTCTGACCC. For PCR amplification, we used 300 ng of DNA in a 25 μl reaction volume containing 0.2 mM of each dNTP, 2 μM of F primer, 1 μM of R primer, 1 μM of R1 primer and 0.5 U/μl Red Taq DNA polymerase (Sigma-Aldrich, Italy). The PCR conditions were as follows: 94 °C for 4 min followed by 37 cycles at 94 °C for 30 s, 58 °C for 30 s, 72 °C for 40 s and a final extension at 72 °C for 7 min. Amplicons were separated using 2% agarose gel and visualized under UV light after staining with Green Gel Plus (Fisher Molecular Biology, Rome, Italy). Amplicon sizes were: WT allele = 462 bp; mutant allele = 371 bp; Cre allele = 310 bp.

Behavioural testing

The testing order for behavioural assessment performed in the same animals consisted of: open field (1 day duration), object recognition test (ORT) at 1h (1 day), ORT at 24h (3 days), Y maze (1 day), Morris water maze (MWM) with hidden platform (7 days), rotarod (1 day), three chamber social test (1 day) and self-grooming (1 day). The mice were tested on one task at a time with the next behavioural test starting at least 1 day after the completion of the previous one. While open field, ORT, Y maze, rotarod and self-grooming were longitudinally administered to the same animals, MWM was performed in separate groups of animals at the different ages tested. Y maze has been also used to test cognitive functions in juvenile animals (P28). Social behaviour has been tested only in 6-month-old animals. In order to reduce the circadian effects, behavioural tests were performed during the same time interval each day (14:00–18:00h; light phase). All behavioural tests were conducted in blind with respect to the genotype of animals. Animals not performing the task required were excluded from the analysis. Mice were weighed at the end of experiments.

Open field and object recognition test (ORT)

The apparatus consisted of a square arena (60 × 60 × 30 cm) constructed in poly(vinyl chloride) with black walls and a white floor. The mice received one session of 10-min duration in the empty arena to habituate them to the apparatus and test room. Animal position was continuously recorded by a video tracking system (Noldus Ethovision XT). In the recording software an area corresponding to the centre of the arena (a central square 30 × 30 cm), and a peripheral region (corresponding to the remaining portion of the arena) were defined. The total movement of the animal and the time spent in the center or in the periphery area were automatically computed. Mouse activity during this habituation session was analysed for evaluating the behaviour in the open field arena. The ORT consisted of two phases: sample and testing phase. During the sample phase, two identical objects were placed in diagonally opposite corners of the arena, approximately 6 cm from the walls, and mice were allowed 10 min to explore the objects, then they were returned to their cage. The objects to be discriminated were made of plastic, metal, or glass material and were too heavy to be displaced

by the mice. The testing phase was performed either 1h or 24h after the sample phase. One of the two familiar objects was replaced with a new one, while the other object was replaced by an identical copy. The objects were placed in the same locations as the previous ones. The mice were allowed to explore objects for 5 min. To avoid possible preferences for one of two objects, the choice of the new and old object and the position of the new one were randomized among animals. The amount of time spent exploring each object (nose sniffing and head orientation within <1.0 cm) was recorded and evaluated by the experimenter blind to the mouse genotype. Arena and objects were cleaned with 10% ethanol between trials to stop the build-up of olfactory cues. Mice exploring the two objects for less than 10 s during the sample phase were excluded from testing. A discrimination index was computed as $DI = (T_{new} - T_{old})/(T_{new} + T_{old})$, where T_{new} is the time spent exploring the new object, and T_{old} is the time spent exploring the old one (11).

Y maze spontaneous alternation

We used a Y-shaped maze with three symmetrical grey solid plastic arms at a 120-degree angle (26 cm length, 10 cm width, and 15 cm height). Mice were placed in the centre of the maze and allowed to freely explore the maze for 8 minutes. The apparatus was cleaned with 10% ethanol between trials to avoid the build-up of odour traces. All sessions were video-recorded (Noldus Ethovision XT) for offline blind analysis. The arm entry was defined as all four limbs within the arm. A triad was defined as a set of three arm entries, when each entry was to a different arm of the maze. The number of arm entries and the number of triads were recorded in order to calculate the alternation percentage (generated by dividing the number of triads by the number of possible alternations and then multiplying by 100; (11)).

Morris water maze

Mice were trained for four trials per day and for a total of 7 days (11) in a circular water tank, made from grey polypropylene (diameter, 120 cm; height, 40 cm), filled to a depth of 25 cm with water (23 °C) rendered opaque by the addition of a non-toxic white paint. Four positions around the edge of the tank were arbitrarily designated North (N), South (S), East (E), and West (W), which provided four alternative start positions and also defined the division of the tank into four quadrants, *i.e.* NE, SE, SW, and NW. A square clear Perspex escape platform (11 × 11 cm) was submerged 0.5 cm below the water surface and placed at the midpoint of one of the four quadrants. The hidden platform remained in the same quadrant during training, while the starting positions (N, S, E, or W) were randomized across trials. The pool was situated in a room containing extra-maze cues that provide specific visual reference points for locating the submerged platform. Mice were allowed up to 60 s to locate the escape platform, and their swimming paths were automatically recorded by the Noldus Ethovision system. If the mouse failed to reach the platform within 60 s, the trial was terminated, and the mouse was guided onto the platform for 15 s. On the last trial of the last training day, mice received a probe trial, during which the escape platform was removed from the tank and the swimming paths were recorded over 60 s while mice searched for the missing platform. The swimming paths were recorded and analysed with the Noldus Ethovision system.

Rotarod

Motor coordination and abilities were assessed using the rotarod test as described in (56). Animals were placed on a drum with increasing rotation speed from 4 to 40 rpm. The time spent on the drum was recorded by an automated unit, which stops as the mouse fall. Motor abilities were assessed by conducting the test for four consecutive times with an interval of 5 min in the same day.

Three-chamber social test

The three-chamber paradigm test has been successfully employed to study sociability and preference for social novelty in several mutant mouse lines. 'Sociability' is defined as a propensity to spend time with a conspecific, as compared to time spent alone in an identical but empty chamber; 'preference for social novelty' is defined as propensity to spend time with a new mouse rather than with a familiar mouse (57). We adapted the protocol reported in (58). The apparatus consisted in a rectangular, three-chamber box made from clear Plexiglas (72 cm wide × 50 cm length × 33 high). Each chamber is 24 x 50 cm and the dividing walls are made from clear Plexiglas, with an open middle section, which allows free access to each chamber. Two identical, wire cup-like containers with removable lids were placed inside the apparatus, one in each side chamber. Each container was made of metal wires allowing for air exchange between the interior and exterior of the cup but small enough to prevent direct physical interactions between the inside animal and the subject mouse. Two classes of mouse were used in this experiment, one acting as a control, naïve animal, while the other is the test subject. The control mouse was a mouse of the same background, age, gender and weight, without any prior contact with the subject mouse. Two control mice were required per experiment, one used for session I (Stranger 1) and another for session II (Stranger 2). The same control mice were used between trials. Control mice were gradually habituated to wire-cup housing in the three-chamber box for 4 days (30 min per day) before the starting of test session. After 10 min of habituation in the arena with empty wire cups of the subject mouse, we placed Stranger 1 inside one of the wire cups. The subject mice were allowed to explore each of the three chambers for 10 min (session I). Animal position was continuously recorded by a video tracking system (Noldus Ethovision XT). The amount of time spent exploring each wire cup was recorded and evaluated by the experimenter blind to the mouse genotype. A discrimination index was computed as DI = (Tsoc - Tobj)/(Tsoc + Tobj), where Tsoc is the time spent exploring the cup housing the Stranger 1, and Tobj is the time spent exploring the other cup. In session II we placed Stranger 2 inside the wire cup in the opposite side chamber. Duration of session II was 10 min and we calculated the same DI described above, differentiating the exploration time of the subject mouse between Stranger 1 and Stranger 2. The placement of Stranger 1 and Stranger 2 in the left or right side of the box was randomized between trials. Arena and wire cups were cleaned with 10% ethanol between trials to prevent olfactory cue bias.

Self-grooming

Mice were scored for spontaneous grooming behaviours as described earlier (59). Each mouse was placed individually into a clean, empty, standard mouse cage (27 length × 20 cm wide × 15 cm high) without bedding. Animal behaviours were

videotaped for 20 min. After a 10-min habituation period in the test cage, each mouse was scored with a stopwatch for 10 min for cumulative time spent grooming all body regions.

Biochemical analysis

For Cr and GAA assay, mouse tissues, immediately frozen on dry ice and stored at -80 °C until the analysis, were homogenized in 0.7 ml PBS buffer (Sigma-Aldrich, Italy) at 4 °C using a ultrasonic disruptor (Microson Heat System, NY, USA) for brain or a glass manual homogenizer (VWR, Italy) for kidney, heart and muscle. After centrifugation (600 × g for 10 min at 4 °C) an aliquot of the homogenate (50 µl) was assayed for protein content and the supernatant used for Cr assay as previously described (60). Briefly, 50 µl of saturated sodium hydrogen carbonate and 50 µl of a mixture containing 2- phenylbutyric acid (I.S.) in toluene (6.09 mmol/l; Sigma-Aldrich, Italy) were added to 200 µl of homogenate or to 100 µl of serum and urine, respectively. After adding 1 ml of toluene and 50 µl of hexafluoro-2,4-pentanedione (Sigma-Aldrich, Italy) to form bistrifluoromethyl- pyrimidine derivatives, the mixture was stirred overnight at 80 °C. The organic layer was centrifuged, dried under nitrogen and 2 µl of the residue derivatized at room temperature with 100 µl of BSTFA + TMCS (Sigma-Aldrich, Italy) injected into the Gas Chromatography/Mass Spectrometry (GC/MS) instrument. GC analyses were performed using an Agilent 6890N GC equipped with an HP5MS capillary column (0.25 mm × 30 m, film thickness 0.25 ìm) and an Agilent mass spectrometer 5973N (Agilent Technologies, Italy). The mass spectrometer was set in EI- single ion monitoring mode (SIM). The ions with m/z of 192 for I.S., 258 for Cr and 225 for guanidinoacetic acid (GAA) were used for calculation of the metabolites, using standard curves ranging 5–90 µmol/l and 0.30–6 µmol/l for Cr and GAA, respectively. Data were processed by the G1701DA MSD ChemStation software. All the aqueous solutions were prepared using ultrapure water produced by a Millipore system.

Immunohistochemistry

Animals were perfused transcardially with 4% paraformaldehyde in phosphate buffer. Brains were post-fixed and impregnated with 30% sucrose in phosphate buffered saline (PBS). Coronal brain sections (40 µm) were cut on a freezing microtome and collected in PBS before being processed for immunohistochemistry. After a blocking step, free-floating slices were incubated O/N at 4 °C in a solution of primary antibody (NeuN, Millipore, 1:500; Ki67, Abcam, 1:400; DCX, Abcam, 1:200; vGlut1, Synaptic System, 1:500; vGAT, Synaptic System, 1:1,000; Iba-1, Wako, 1:400) and antigen-antibody interaction was revealed with suitable Alexa Fluor-conjugated secondary antibodies (1:400, Invitrogen). Immunostaining for Ki67 involved an additional treatment with sodium citrate for antigen retrieval. Sections were then counterstained with Hoechst dye (1:500, Sigma), mounted on microscope slides and coverslipped using Vectashield mounting medium for fluorescence (Vector Laboratories Inc.).

Image analysis

NeuN and Iba1- To quantify the density of neuronal and microglial cells in the cerebral cortex we used the StereoInvestigator software (MicroBrightField) equipped with motorized X–Y sensitive stage and video camera connected to a computerized image analysis system. NeuN-positive cells were counted using 20x magnification and sampling boxes (250 × 250 × 40 µm) located in both superficial and deep layers of PFC and ACC cortex. Iba1-positive cells were counted using 40x magnification and sampling boxes (250 × 250 × 40 µm) located in both superficial and deep layers of PFC cortex. Cell density was calculated by averaging values obtained from at least 6-8 counting boxes per animal. *Ki67 and DCX*- Examination of Ki67 and DCX-positively labelled cells was confined to the hippocampal dentate gyrus (DG), specifically to the granule cell layer (GCL) and the subgranular zone of the hippocampus defined as a two-cell body-wide zone along the border between the GCL and hilus. Quantification of Ki67 or DCX-immunoreactive cells was conducted from 1-in-6 series of immunolabelled sections using 20x magnification and spanning the rostrocaudal extent of DG. All immunostained sections were analysed using the StereoInvestigator software. The reference volume was determined as the sum of the traced areas multiplied by the distance between the sampled sections. Densities of immunopositive cells were then calculated by dividing the number of positive cells by the reference volume. Numbers of positively labelled neurons were normalized as density per unit of volume (mm^3). *vGlut1 and vGAT*- To quantify the density of vGlut1- and vGAT-positive puncta, the parameters of acquisition (laser intensity, gain, offset) were optimized at the beginning of the acquisition and then held constant throughout image acquisition. All sections were acquired in random order in a single session to minimize fluctuation in laser output and degradation of fluorescence. We imaged superficial and deep layers of PFC and ACC on a Zeiss laser-scanning Apotome microscope using a 63x oil immersion objective. For each section, we imaged serial optical sections at 0.33 µm intervals for a total of at least 15 optical sections (5 µm). From each animal we imaged 6 sections (3 in superficial layers and 3 in deep layers). Maximum intensity projections (MIPs) were generated from the group of 5 consecutive sections yielding the higher mean pixel intensity. These MIPs were imported in ImageJ and quantified using Puncta analyzer plugin (61). The number of positive puncta was measured within the entire acquired area.

Determination of lipofuscin accumulation by autofluorescence

Coronal brain sections were mounted on microscope slides and coverslipped using Vectashield mounting medium for fluorescence (Vector Laboratories Inc.). We imaged hippocampal DG on a Zeiss laser-scanning Apotome microscope using a 40× oil immersion objective. The parameters of acquisition were optimized at the beginning of the experiment and then held constant. Lipofuscin level was measured as the presence of autofluorescence at 550 nm in the region of interest. For each section, we imaged serial optical sections at 0.5 µm intervals for a total of at least 80 optical sections (40 µm). From each animal we imaged 3–4 sections. MIPs were generated from the group of 5 consecutive sections yielding the higher mean pixel intensity. These MIPs were imported in ImageJ and quantified using Threshold plugin. The area of positive puncta and mean pixel intensity were measured within the entire acquired area.

Statistical analysis

All statistical analyses were performed using SigmaStat Software. Differences between two groups were assessed with a

two-tailed *t* test. The significance of factorial effects and differences among more than two groups were evaluated with ANOVA/RM ANOVA followed by Holm-Sidak test. Rank transformation was exploited for data not normally distributed. The level of significance was $P < 0.05$.

Supplementary Material

Supplementary Material is available at *HMG* online.

Acknowledgements

We thank Francesca Biondi for animal care and Cristina Pitzalis for test representative illustrations.

Conflict of Interest statement. None declared.

Funding

This work has been supported by Neuroscience Institute of CNR and University of Florence.

References

1. Wallimann, T., Tokarska-Schlattner, M. and Schlattner, U. (2011) The creatine kinase system and pleiotropic effects of creatine. *Amino Acids*, **40**, 1271–1296.
2. Joncquel-Chevalier Curt, M., Voicu, P.M., Fontaine, M., Dessein, A.F., Porchet, N., Mention-Mulliez, K., Dobbelaere, D., Soto-Ares, G., Cheillan, D. and Vamecq, J. (2015) Creatine biosynthesis and transport in health and disease. *Biochimie*, **119**, 146–165.
3. Item, C.B., Stöckler-Ipsiroglu, S., Stromberger, C., Mühl, A., Alessandrì, M.G., Bianchi, M.C., Tosetti, M., Fornai, F. and Cioni, G. (2001) Arginine:glycine amidinotransferase deficiency: the third inborn error of creatine metabolism in humans. *Am. J. Hum. Genet.*, **69**, 1127–1133.
4. Stöckler, S., Holzbach, U., Hanefeld, F., Marquardt, I., Helms, G., Requart, M., Hänicke, W. and Frahm, J. (1994) Creatine deficiency in the brain: a new, treatable inborn error of metabolism. *Pediatr. Res.*, **36**, 409–413.
5. Salomons, G.S., van Dooren, S.J., Verhoeven, N.M., Cecil, K.M., Ball, W.S., Degrauw, T.J. and Jakobs, C. (2001) X-linked creatine-transporter gene (SLC6A8) defect: a new creatine-deficiency syndrome. *Am. J. Hum. Genet.*, **68**, 1497–1500.
6. van de Kamp, J.M., Mancini, G.M. and Salomons, G.S. (2014) X-linked creatine transporter deficiency: clinical aspects and pathophysiology. *J. Inherit. Metab. Dis.*, **37**, 715–733.
7. Mak, C.S.W., Waldvogel, H.J., Dodd, J.R., Gilbert, R.T., Lowe, M.T.J., Birch, N.P., Faull, R.L.M. and Christie, D.L. (2009) Immunohistochemical localisation of the creatine transporter in the rat brain. *Neuroscience*, **163**, 571–585.
8. Braissant, O., Henry, H., Béard, E. and Uldry, J. (2011) Creatine deficiency syndromes and the importance of creatine synthesis in the brain. *Amino Acids*, **40**, 1315–1324.
9. Torremans, A., Marescau, B., Possemiers, I., Van Dam, D., D'Hooge, R., Isbrandt, D. and De Deyn, P.P. (2005) Biochemical and behavioural phenotyping of a mouse model for GAMT deficiency. *J. Neurol. Sci.*, **231**, 49–55.
10. Skelton, M.R., Schaefer, T.L., Graham, D.L., Degrauw, T.J., Clark, J.F., Williams, M.T. and Vorhees, C.V. (2011) Creatine transporter (CrT; Slc6a8) knockout mice as a model of human CrT deficiency. *PLoS One*, **6**, e16187.
11. Baroncelli, L., Alessandrì, M.G., Tola, J., Putignano, E., Migliore, M., Amendola, E., Gross, C., Leuzzi, V., Cioni, G. and Pizzorusso, T. (2014) A novel mouse model of creatine transporter deficiency. *F1000Res.*, **3**, 228.
12. Choe, C.U., Nabuurs, C., Stockebrand, M.C., Neu, A., Nunes, P., Morellini, F., Sauter, K., Schillemeit, S., Hermans-Borgmeyer, I., Marescau, B., *et al.* (2013) L-arginine:glycine amidinotransferase deficiency protects from metabolic syndrome. *Hum. Mol. Genet.*, **22**, 110–123.
13. Nabuurs, C.I., Choe, C.U., Veltien, A., Kan, H.E., van Loon, L.J.C., Rodenburg, R.J.T., Matschke, J., Wieringa, B., Kemp, G.J., Isbrandt, D., *et al.* (2013) Disturbed energy metabolism and muscular dystrophy caused by pure creatine deficiency are reversible by creatine intake. *J. Physiol.*, **591**, 571–592.
14. Alcaide, P., Merinero, B., Ruiz-Sala, P., Richard, E., Navarrete, R., Arias, A., Ribes, A., Artuch, R., Campistol, J., Ugarte, M., *et al.* (2011) Defining the pathogenicity of creatine deficiency syndrome. *Hum. Mutat.*, **32**, 282–291.
15. Bender, A., Beckers, J., Schneider, I., Hölter, S.M., Haack, T., Ruthsatz, T., Vogt-Weisenhorn, D.M., Becker, L., Genius, J., Rujescu, D., *et al.* (2008) Creatine improves health and survival of mice. *Neurobiol. Aging*, **29**, 1404–1411.
16. Lawler, J.M., Barnes, W.S., Wu, G., Song, W. and Demaree, S. (2002) Direct antioxidant properties of creatine. *Biochem. Biophys. Res. Commun.*, **290**, 47–52.
17. Sestili, P., Martinelli, C., Colombo, E., Barbieri, E., Potenza, L., Sartini, S. and Fimognari, C. (2011) Creatine as an antioxidant. *Amino Acids*, **40**, 1385–1396.
18. McMorris, T., Mielcarz, G., Harris, R.C., Swain, J.P. and Howard, A. (2007) Creatine supplementation and cognitive performance in elderly individuals. *Neuropsychol. Dev. Cogn. B Aging Neuropsychol. Cogn.*, **14**, 517–528.
19. van de Kamp, J.M., Betsalel, O.T., Mercimek-Mahmutoglu, S., Abulhoul, L., Grünewald, S., Anselm, I., Azzouz, H., Bratkovic, D., de Brouwer, A., Hamel, B., *et al.* (2013) Phenotype and genotype in 101 males with X-linked creatine transporter deficiency. *J. Med. Genet.*, **50**, 463–472.
20. Laakso, M.P., Hiltunen, Y., Könönen, M., Kivipelto, M., Koivisto, A., Hallikainen, M. and Soininen, H. (2003) Decreased brain creatine levels in elderly apolipoprotein E epsilon 4 carriers. *J. Neural Transm.*, **110**, 267–275.
21. Smith, R.N., Agharkar, A.S. and Gonzales, E.B. (2014) A review of creatine supplementation in age-related diseases: more than a supplement for athletes. *F1000Res.*, **3**, 222.
22. Albani, S.H., McHail, D.G. and Dumas, T.C. (2014) Developmental studies of the hippocampus and hippocampal-dependent behaviors: Insights from interdisciplinary studies and tips for new investigators. *Neurosci. Biobehav. Rev.*, **43**, 183–190.
23. Etherton, M.R., Blaiss, C.A., Powell, C.M. and Sudhof, T.C. (2009) Mouse neurexin-1 deletion causes correlated electrophysiological and behavioral changes consistent with cognitive impairments. *Proceedings of the National Academy of Sciences*, **106**, 17998–18003.
24. Rothwell, P.E., Fuccillo, M.V., Maxeiner, S., Hayton, S.J., Gokce, O., Lim, B.K., Fowler, S.C., Malenka, R.C. and Südhof, T.C. (2014) Autism-associated neuroligin-3 mutations commonly impair striatal circuits to boost repetitive behaviors. *Cell*, **158**, 198–212.
25. Fuccillo, M.V. (2016) Striatal Circuits as a Common Node for Autism Pathophysiology. *Front. Neurosci.*, **10**, 27.
26. Bano, D., Agostini, M., Melino, G. and Nicotera, P. (2011) Ageing, neuronal connectivity and brain disorders: an unsolved ripple effect. *Mol. Neurobiol.*, **43**, 124–130.
27. Leuzzi, V., Mastrangelo, M., Battini, R. and Cioni, G. (2013) Inborn errors of creatine metabolism and epilepsy. *Epilepsia*, **54**, 217–227.

28. von Bernhardi, R., Eugenín-von Bernhardi, L. and Eugenín, J. (2015) Microglial cell dysregulation in brain aging and neurodegeneration. *Front. Aging Neurosci.*, **7**, 124.
29. Matt, S.M. and Johnson, R.W. (2016) Neuro-immune dysfunction during brain aging: new insights in microglial cell regulation. *Curr. Opin. Pharmacol.*, **26**, 96–101.
30. Hefendehl, J.K., Neher, J.J., Sühs, R.B., Kohsaka, S., Skodras, A. and Jucker, M. (2014) Homeostatic and injury-induced microglia behavior in the aging brain. *Aging Cell*, **13**, 60–69.
31. Lee, S.W., Clemenson, G.D. and Gage, F.H. (2012) New neurons in an aged brain. *Behav. Brain Res.*, **227**, 497–507.
32. Dunlop, R.A., Brunk, U.T. and Rodgers, K.J. (2009) Oxidized proteins: mechanisms of removal and consequences of accumulation. *IUBMB Life*, **61**, 522–527.
33. Terman, A. and Brunk, U.T. (2006) Oxidative stress, accumulation of biological 'garbage', and aging. *Antioxid. Redox Signal.*, **8**, 197–204.
34. Assunção, M., Santos-Marques, M.J., Carvalho, F., Lukoyanov, N.V. and Andrade, J.P. (2011) Chronic green tea consumption prevents age-related changes in rat hippocampal formation. *Neurobiol. Aging*, **32**, 707–717.
35. Tronche, F., Kellendonk, C., Kretz, O., Gass, P., Anlag, K., Orban, P.C., Bock, R., Klein, R. and Schütz, G. (1999) Disruption of the glucocorticoid receptor gene in the nervous system results in reduced anxiety. *Nat. Genet*, **23**, 99–103.
36. Puusepp, H., Kall, K., Salomons, G.S., Talvik, I., Männamaa, M., Rein, R., Jakobs, C. and Õunap, K. (2010) The screening of SLC6A8 deficiency among Estonian families with X-linked mental retardation. *J Inherit Metab Dis*, **33**, S5–11.
37. Matthews, R.T., Ferrante, R.J., Klivenyi, P., Yang, L., Klein, A.M., Mueller, G., Kaddurah-Daouk, R. and Beal, M.F. (1999) Creatine and cyclocreatine attenuate MPTP neurotoxicity. *Exp. Neurol.*, **157**, 142–149.
38. Sullivan, P.G., Geiger, J.D., Mattson, M.P. and Scheff, S.W. (2000) Dietary supplement creatine protects against traumatic brain injury. *Ann. Neurol.*, **48**, 723–729.
39. O'Gorman, E., Beutner, G., Dolder, M., Koretsky, A.P., Brdiczka, D. and Wallimann, T. (1997) The role of creatine kinase in inhibition of mitochondrial permeability transition. *FEBS Lett.*, **414**, 253–257.
40. Kempermann, G. (2015) Activity Dependency and Aging in the Regulation of Adult Neurogenesis. *Cold Spring Harb. Perspect. Biol.*, **7**.
41. Bartsch, T. and Wulff, P. (2015) The hippocampus in aging and disease: From plasticity to vulnerability. *Neuroscience*, **309**, 1–16.
42. Christian, K.M., Song, H. and Ming, G.L. (2014) Functions and dysfunctions of adult hippocampal neurogenesis. *Annu. Rev. Neurosci.*, **37**, 243–262.
43. Bories, C., Husson, Z., Guitton, M.J. and De Koninck, Y. (2013) Differential balance of prefrontal synaptic activity in successful versus unsuccessful cognitive aging. *J. Neurosci.*, **33**, 1344–1356.
44. McQuail, J.A., Frazier, C.J. and Bizon, J.L. (2015) Molecular aspects of age-related cognitive decline: the role of GABA signaling. *Trends Mol. Med.*, **21**, 450–460.
45. Rao, J.S., Matthew, K., Hyung-Wook, K., Rapoport, S.I. and Reese, E.A. (2012) Neuroinflammation and Synaptic Loss. *Neurochem. Res.*, **37**, 903–910.
46. Rao, J.S., Kim, H.W., Kellom, M., Greenstein, D., Chen, M., Kraft, A.D., Harry, G.J., Rapoport, S.I. and Basselin, M. (2011) Increased neuroinflammatory and arachidonic acid cascade markers, and reduced synaptic proteins, in brain of HIV-1 transgenic rats. *J. Neuroinflammation*, **8**, 101.
47. Kellom, M., Basselin, M., Keleshian, V.L., Chen, M., Rapoport, S.I. and Rao, J.S. (2012) Dose-dependent changes in neuroinflammatory and arachidonic acid cascade markers with synaptic marker loss in rat lipopolysaccharide infusion model of neuroinflammation. *BMC Neurosci.*, **13**, 50.
48. Sierra, A., Beccari, S., Diaz-Aparicio, I., Encinas, J.M., Comeau, S. and Tremblay, M. (2014) Surveillance, phagocytosis, and inflammation: how never-resting microglia influence adult hippocampal neurogenesis. *Neural Plast.*, **2014**, 610343.
49. Ryan, S.M. and Nolan, Y.M. (2016) Neuroinflammation negatively affects adult hippocampal neurogenesis and cognition: can exercise compensate? *Neurosci. Biobehav. Rev.*, **61**, 121–131.
50. Höhn, A. and Grune, T. (2013) Lipofuscin: formation, effects and role of macroautophagy. *Redox Biol*, **1**, 140–144.
51. Brandenstein, L., Schweizer, M., Sedlacik, J., Fiehler, J. and Storch, S. (2016) Lysosomal dysfunction and impaired autophagy in a novel mouse model deficient for the lysosomal membrane protein Cln7. *Hum. Mol. Genet.*, **25**, 777–791.
52. Kopra, O., Vesa, J., von Schantz, C., Manninen, T., Minye, H., Fabritius, A.L., Rapola, J., van Diggelen, O.P., Saarela, J., Jalanko, A., *et al.* (2004) A mouse model for Finnish variant late infantile neuronal ceroid lipofuscinosis, CLN5, reveals neuropathology associated with early aging. *Hum. Mol. Genet.*, **13**, 2893–2906.
53. Ahmed, Z., Sheng, H., Xu, Y.F., Lin, W.L., Innes, A.E., Gass, J., Yu, X., Wuertzer, C.A., Hou, H., Chiba, S., *et al.* (2010) Accelerated lipofuscinosis and ubiquitination in granulin knockout mice suggest a role for progranulin in successful aging. *Am. J. Pathol.*, **177**, 311–324.
54. Maccarinelli, F., Pagani, A., Cozzi, A., Codazzi, F., Di Giacomo, G., Capoccia, S., Rapino, S., Finazzi, D., Politi, L.S., Cirulli, F., *et al.* (2015) A novel neuroferritinopathy mouse model (FTL 498InsTC) shows progressive brain iron dysregulation, morphological signs of early neurodegeneration and motor coordination deficits. *Neurobiol. Dis.*, **81**, 119–133.
55. Head, E., Lott, I.T., Wilcock, D.M. and Lemere, C.A. (2016) Aging in Down Syndrome and the Development of Alzheimer's Disease Neuropathology. *Curr. Alzheimer Res.*, **13**, 18–29.
56. Lonetti, G., Angelucci, A., Morando, L., Boggio, E.M., Giustetto, M. and Pizzorusso, T. (2010) Early environmental enrichment moderates the behavioral and synaptic phenotype of MeCP2 null mice. *Biol. Psychiatry*, **67**, 657–665.
57. Moy, S.S., Nadler, J.J., Perez, A., Barbaro, R.P., Johns, J.M., Magnuson, T.R., Piven, J. and Crawley, J.N. (2004) Sociability and preference for social novelty in five inbred strains: an approach to assess autistic-like behavior in mice. *Genes Brain Behav.*, **3**, 287–302.
58. Kaidanovich-Beilin, O., Lipina, T., Vukobradovic, I., Roder, J. and Woodgett, J.R. (2011) Assessment of social interaction behaviors. *J. Vis. Exp*, 10.3791/2473.
59. McFarlane, H.G., Kusek, G.K., Yang, M., Phoenix, J.L., Bolivar, V.J. and Crawley, J.N. (2008) Autism-like behavioral phenotypes in BTBR T+tf/J mice. *Genes Brain Behav.*, **7**, 152–163.
60. Alessandrì, M.G., Celati, L., Battini, R., Casarano, M. and Cioni, G. (2005) Gas chromatography/mass spectrometry assay for arginine: glycine-amidinotransferase deficiency. *Anal. Biochem.*, **343**, 356–358.
61. Ippolito, D.M. and Eroglu, C. (2010) Quantifying synapses: an immunocytochemistry-based assay to quantify synapse number. *J. Vis. Exp*, 10.3791/2270.